Journal of Solid State Electrochemistry (2022) 26:1399–1407
https://doi.org/10.1007/s10008-022-05171-5

ORIGINAL PAPER

Research on the electrochromic properties of Mxene intercalated vanadium pentoxide xerogel films

Danrui Yu[1] · Wei Wei[1,3] · Min Wei[1,2] · Fei Wang[1] · Xiao Liang[1] · Shuokun Sun[1,2] · Mingrui Gao[1,2] · Quanyao Zhu[1]

Received: 9 February 2022 / Revised: 16 March 2022 / Accepted: 11 April 2022 / Published online: 5 May 2022

Abstract

Vanadium pentoxide (V_2O_5) is one of the most popular electrochromic material for electrochromic devices due to its excellent storage capacity of lithium ions and unique properties of anodic/cathodic coloring. However, V_2O_5 generally has low conductivity, causing a long coloration/bleaching response time. Consequently, its practical use as a electrochromic material in practical industrial applications remains limited. In this paper, V_2O_5/Mxene intercalation films (VOM) were prepared by sol–gel method with spin-coating technology. The structure and morphology of the intercalation films were characterized by X-ray diffraction (XRD), X-ray photoelectron spectroscopy (XPS), field-emission scanning electron microscopy (FESEM), and other testing techniques. The optical properties of the films were characterized by ultraviolet–visible (UV–Vis) spectroscopy, and the electrochemical properties were analyzed by cyclic voltammetry (CV) and chronoamperometry (CA). The results showed that the Mxene intercalation of V_2O_5 xerogel widened the interplanar distance. The bleaching time of the intercalation films was 3.20 s and the coloring time was 6.20 s when the Mxene doping was 3 wt%. Meanwhile, the transmittance contrast increased from 7.70 to 49.03% at 372 nm compared with the V_2O_5 xerogel films.

Keywords V_2O_5/Mxene · Sol–gel method · Electrochromic properties

Introduction

Electrochromism is the reversible change of the optical properties of a material under the action of an applied alternating voltage [1]. Electrochromic materials have a wide range of applications, including smart windows, anti-glare car mirrors, military camouflage and, electrochromic displays. [2–10]. Electrochromic materials can be classified into inorganic electrochromic materials, organic electrochromic materials, and composite electrochromic materials. Compared with the organic electrochromic materials, the inorganic electrochromic materials exhibit better thermal and chemical stability, and therefore, their commercial applications are more valuable [11–14].

Among the transition metal oxides, vanadium oxides are the only electrochromic materials with anodic and cathodic coloring properties that have been found so far, which can achieve a blue-green-yellow color transition by ion insertion/extraction processes. In addition, V_2O_5 gels are receiving more and more attention because of their layered structure and large theoretical charge capacity (~ 294 mAh g^{-1}) [15, 16]. However, their poor electrical conductivity (~ 10^{-2}–10^{-3} S cm^{-1}) [17, 18], low diffusion coefficient of lithium ions (~ 10^{-12} cm^2 s^{-1}) [19, 20], and structural phase transitions during redox can cause lattice strain, leading to irreversible structural damage and ultimately irreversible capacity loss, which limits its practical application. Researchers have compounded additional materials such as carbides, metal oxides, and conducting polymers with V_2O_5 gels [21–26], which can improve the electrical conductivity of the materials and effectively improve their electrochromic properties.

Mxene is a general term for transition metal carbides, nitrides, and carbon–nitrogen compounds and is one of the most promising members of two-dimensional

✉ Quanyao Zhu
cglamri@whut.edu.cn

Danrui Yu
danruiyu@whut.edu.cn

[1] School of Materials Science and Engineering, Wuhan University of Technology, Wuhan 430070, Hubei, China

[2] Henan Key Laboratory of Special Protective Materials, Luoyang 471023, Henan, China

[3] Department of Physics, Changji University, Changji 831100, Xinjiang, China

materials for research [27]. The chemical formula of Mxene is generally written as $M_{n+1}X_nT_x$ ($n = 1, 2, 3$), where *M* represents transition metal elements (such as Ti, V, W), *X* represents C or N, and T_x stands for the various possible terminations (e.g., -OH, -O, or -F). The two-dimensional lamellar structure of Mxene has received much attention due to its large specific surface area, excellent electrical conductivity (~ $8*10^3$–$10*10^3$ S cm^{-1}), high mechanical properties, and more stable chemical properties [28–30]. Mxene can be compounded with V_2O_5 by hydrothermal and physical ultrasonic stirring [31]. The confinement between Mxene sheets by V_2O_5 can effectively prevent aggregation, stacking, oxidation, and degradation during charge/discharge cycles. Mxene can reduce the charge transport potential of V_2O_5. For example, the three-dimensional hydrated V_2O_5/Mxene composite prepared by hydrothermal method has a large specific surface area and high structural stability, which elevate the rate capacity (its specific capacity is 323 mAh g^{-1} at a current density of 0.1 A g^{-1}) when used as cathode material for aqueous zinc ion batteries [32]. The two-dimensional heterostructure of V_2O_5/Mxene aqueous composite ink prepared by self-assembly, combined with an inkjet printer for lithium-ion battery cathode material, has good cycling stability and high specific capacitance (91.7% capacity retention and 96.5% coulombic efficiency after 680 cycles at a discharge rate of 10.5 C) [33]. The V_2O_5/Mxene@CC prepared by ultrasonication has an excellent specific capacity (its specific capacity is 768 F g^{-1} at a current density of 0.1 A g^{-1}) and good cycling performance (93.3% specific capacity was maintained after completing 6000 constant current charge and discharge tests) when used as a working electrode in a half-cell configuration [34]. The above studies fully demonstrate the potential of V_2O_5/Mxene composites in the field of electrochemistry. However, V_2O_5/Mxene composites have not been reported in electrochromic studies in the same field of electrochemistry. On the other hand, V_2O_5/Mxene intercalated films are more focused on the effect of optical modulation and the study of electrochemical-optical relationships can better provide theoretical data for their electrochemical performance studies. For these reasons, it can be expected that intercalation of Mxene into V_2O_5 gels can lead to homogeneous films suitable for electrochromic devices.

In this paper, V_2O_5 sols were prepared by Livage's Method [35], and the composite sols were obtained by ultrasonically making Mxene fully dispersed in V_2O_5 sols, and the intercalated films were prepared on indium tin oxide (ITO) coated substrates by spin coating method and heat treated at 180 °C. The structural, morphological, electrochemical, and optical properties of Mxene intercalated V_2O_5 xerogel films were investigated.

Experimental

Materials

All chemical reagents used are analytically pure; no further purification is required. V_2O_5 was purchased from Shanghai Shanpu Chemical Co. Ltd (China), 30% hydrogen peroxide (H_2O_2) solution, sodium hydroxide (NaOH), acetone, ethanol, propylene carbonate (PC), and lithium perchlorate trihydrate ($LiClO_4{\cdot}3H_2O$) were supplied by Sinopharm Chemical Reagent Co. Ltd (China). Single-layer Mxene dispersion with a solubility of 4 mg/mL ($Ti_3C_2T_x$, based on Fig. S1 FTIR spectra T_x = -O, -OH, -F,) was purchased from Hangzhou Nano-Mall Technology Co. Ltd. (China). The thickness of $Ti_3C_2T_x$ nanosheets is 1.5 nm. Figure S2 shows the XRD patterns of V_2O_5 powder; all diffraction peaks of the V_2O_5 powder detected are consistent with orthorhombic V_2O_5 (JCPDS #41–1426). The XRD data of the spin-coated Mxene film is displayed in Fig. S3 and agrees well with the literature [33]. In addition, the TEM images of (a) V2O5 powders and (b) single-layer Mxene dispersion can be referred to Fig. S4.

V_2O_5/Mxene composite suspension

Weigh 3.64 g of V_2O_5 powder as a vanadium precursor dispersed in 184.0 mL of deionized water, slowly add 16.0 mL of 30% H_2O_2 dropwise to the V_2O_5 suspension, stir uniformly for 30 mins, and then sonicate for 8 h to obtain brown V_2O_5 sol. The single-layer Mxene dispersion was mixed with a certain amount of V_2O_5 sol at a ratio of 0,1, 2, 3, 4, and 5 wt% of Mxene relative to V_2O_5 precursor, and the dispersion was sonicated for 20 mins by an ultrasonic cell crusher to obtain a homogeneous V_2O_5/Mxene composite suspension. Figure S5 shows TEM images of (a) V_2O_5 sol and (b) V_2O_5/Mxene (3%) suspension. We took a drop of samples on the micro-grids and thoroughly dried those before the TEM studies. Figure S5a shows that the morphology of the particles in the V_2O_5 sol is nanowire-like with an average width of 15 nm and a length spanning micrometers. Figure S5b shows that the morphology of vanadium pentoxide in the V_2O_5/Mxene (3%) suspension is also nanowire-like with an average width of 5 nm and a length spanning micrometers, while that of Mxene is in the form of a monolayer of nanosheets. The particles in the suspension are more neatly arranged. The images of the Tyndall effect in Fig. S6 show the good dispersion of V_2O_5 and V_2O_5/Mxene composite in deionized water, which is favorable to the formation of uniform films [36].

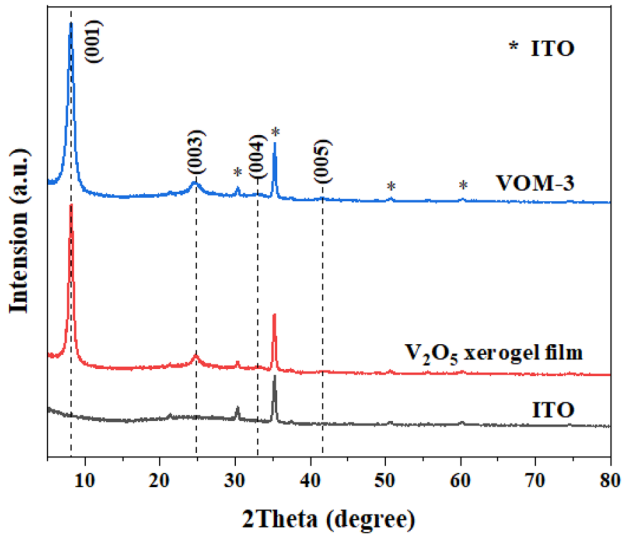

Fig. 1 XRD patterns of V_2O_5 xerogel film and VOM-3 on ITO substrate

V_2O_5/Mxene intercalation films

The ITO glass used in the experiments is 40.0-mm long, 10.0-mm wide, and 1.1-mm thick, with a square resistance of about 7.0 Ω sq^{-1}. Before coating, it needs to be cleaned to remove the surface stains of ITO glass and to ensure the uniformity and adhesion of the film. The specific operation is as follows: the ITO glass was immersed and sonicated for 15 min in 0.5 mol/L NaOH solution, acetone, ethanol, and deionized water in turn, and then placed in a petri dish to dry at room temperature. The V_2O_5/Mxene composite suspension was spin-coated on the ITO glass three times at 3000 rpm/s, dried at room temperature, and then placed in an electric constant temperature oven and heat-treated at 180 °C for 24 h to obtain a uniform V_2O_5/Mxene intercalation film. The films were named as VOM-1, VOM-2, VOM-3, VOM-4, and VOM-5 according to the mass content of Mxene in vanadium precursor of 1, 2, 3, 4, and 5 wt%, respectively.

Characterization

The crystal structure of the films were characterized by XRD (Empyrean, PANalytical, the Netherlands) by using Cu-Kα (Kα = 1.5418 Å) radiation. XPS (ESCALAB 250Xi, Thermo Fisher Scientific, USA) was used to analyze the valence states of the elements. The surface morphology of the films was observed by FESEM with a built-in EDS capability (JSM-7500F, JEOL, Japan) and atomic force microscopy (AFM) (Nanoscope IV, VEECO, USA) measurements were done on 5 μm * 5 μm sample's area and the detection principle is tapping mode. The microstructure of samples was analyzed by TEM (JEM-1400Plus, JEOL, Japan). The transmittance and absorptivity spectra of the films under different polarization voltages were recorded ex situ on a UV–Vis spectrophotometer (Lambda 750 S, PerkinElmer, USA), and the optical band gap of the films was calculated.

All the electrochemical measurements were performed in a three-electrode cell configuration with the electrochemical workstation (IviumStart, IVIUM, the Netherlands). CV and CA were performed using a three-electrode cell configuration. The films prepared on ITO glass were used as the working electrode, the platinum electrode was used as the counter electrode, and the saturated calomel electrode was used as the reference electrode. The electrolyte solution was made of 1 M $LiClO_4$ dissolved in PC. The voltage scanning range of CV was −1.0 V to approximately 1.0 V,

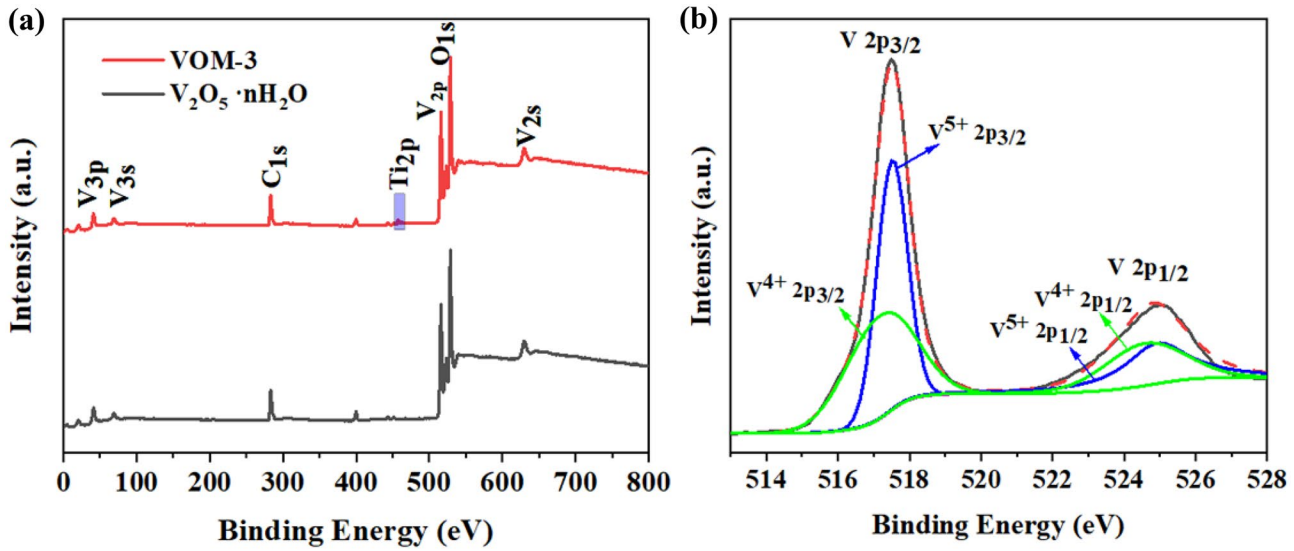

Fig. 2 (**a**) XPS patterns of the V_2O_5 xerogel film and VOM-3, (**b**) high-resolution XPS spectra of V 2p of VOM-3

and the scanning rate was 50 mV s^{-1}. CA applied voltages of −1.0 V and 1.0 V with an interval period of 30 s.

Results and discussion

Morphology and structure

Figure 1 shows the XRD patterns of V_2O_5 xerogel film and VOM-3 deposited on ITO glass after heat treatment. The diffraction peaks of the V_2O_5 xerogel film at 8.18°, 24.69°, 33.29°, and 41.54° correspond to the (001), (003), (004), and (005) crystal planes of $V_2O_5{\cdot}nH_2O$, respectively, and the phase structure of the films is typical of the V_2O_5 xerogel films of $V_2O_5.nH_2O$ [37–39]. The diffraction peaks of V_2O_5 xerogel film are strong and narrow, indicating that the film is highly crystalline. The strongest peak is shifted to a lower angle compared to the V_2O_5 xerogel films for VOM-3, and by using the Bragg–Brentano equation: $2d\sin\theta = n\lambda$, where d is the interlayer distance, θ is half of the diffraction angle, n is the diffraction order, and λ is the wavelength of the X-ray. The interplanar distance can be calculated as 10.81 Å

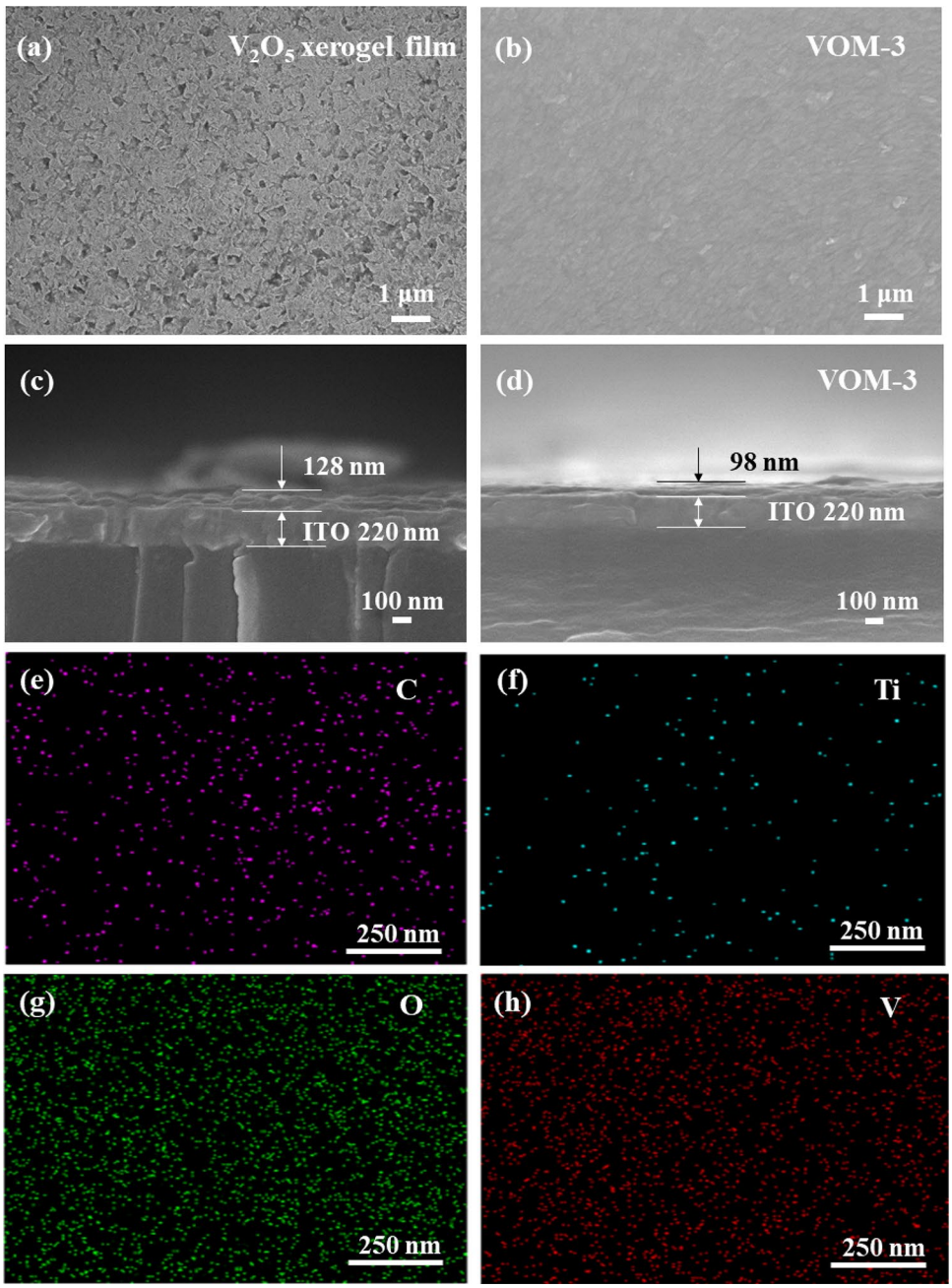

Fig. 3 Surface FESEM images of (**a**) V_2O_5 xerogel film, (**b**) VOM-3. Cross-sections FESEM images of (**c**) V_2O_5 xerogel film, (**d**) VOM-3. (**e–h**) EDS mapping images of VOM-3

for the V_2O_5 xerogel films and 10.87 Å for VOM-3. In addition, the diffraction peaks of VOM-3 become wider, indicating that Mxene, in addition to being embedded between the V_2O_5 xerogel layers, leads to a decrease in the crystallinity of the intercalated films in the c-axis.

Figure 2a shows the XPS patterns of V_2O_5 xerogel film and VOM-3. The general XPS survey spectrum of V_2O_5 xerogel film shows V and O peaks. For VOM-3, peaks corresponding to V, O, C, and Ti are detected, which confirms that V_2O_5 and Mxene hybrids were successfully synthesized. The regional XPS spectra were all calibrated with the binding energy of the adventitious C 1 s peak. Figure 2b shows the high-resolution XPS spectra of V 2p, it can be divided into two obvious peaks located at 517.50 eV and 525.10 eV, referring to V $2p_{3/2}$ and V $2p_{1/2}$ of V_2O_5, respectively. In the V $2p_{3/2}$ level, V^{4+} and V^{5+} was positioned at binding energies of 517.18 eV and 517.52 eV [40]. What is more, the content ratio of V^{5+} and V^{4+} can be determined as 5:4 by the peak area at V $2p_{3/2}$.

Figure 3 shows the surface FESEM images of (a) V_2O_5 xerogel film and (b) VOM-3. The V_2O_5 xerogel film is a porous mesh structure, which may be formed due to dehydration during the heat treatment of the xerogel. In contrast, the surface of VOM-3 is uniform with no obvious holes, cracks, and other types of defects. From AFM analysis (Fig. S7), it is possible to observe roughness images of (a) V_2O_5 xerogel film and (b) VOM-3 generated by the Nano Scope Analysis. The root mean square (RMS) roughness of V_2O_5 xerogel film is 3.51 nm, while the RMS of VOM-3 is 3.24 nm. Figure 3 shows the cross-sections FESEM images of the (c) V_2O_5 xerogel film and (d) VOM-3, the thickness of the V_2O_5 xerogel film is about 128 nm, and the thickness

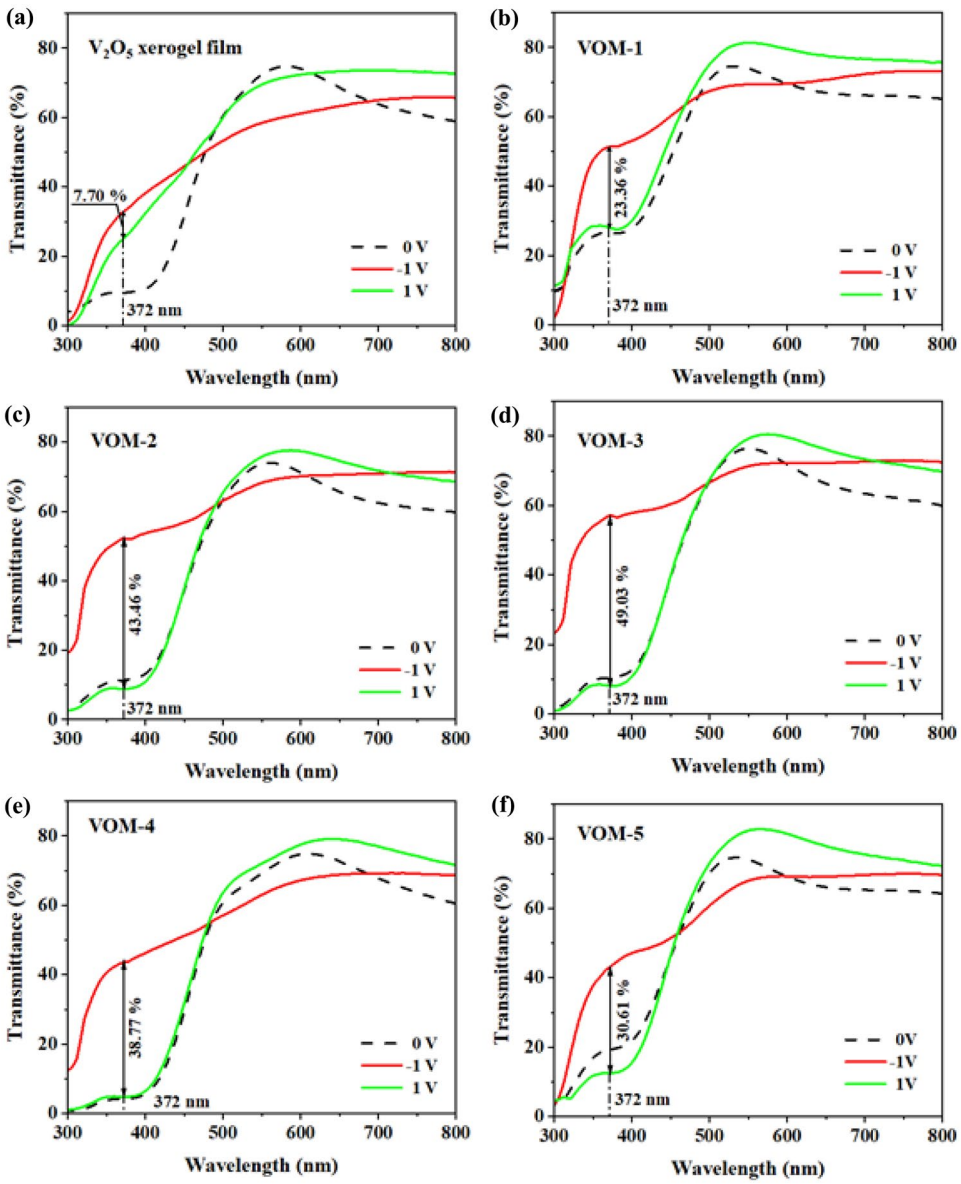

Fig. 4 Ex situ transmittance spectra at bleached/colored states of (**a**) V_2O_5 xerogel film, (**b**) VOM-1, (**c**) VOM-2, (**d**) VOM-3, (**e**) VOM-4, and (**f**) VOM-5

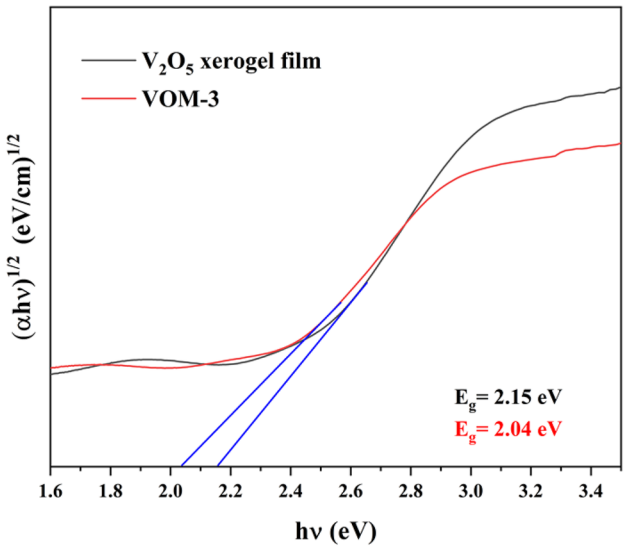

Fig. 5 Energy gap of V_2O_5 xerogel film and VOM-3

of VOM-3 is about 98 nm. In addition, Fig. 3e–h shows the EDS mapping images of VOM-3. As shown in the figure, the V, O, C, and Ti elements are uniformly distributed, which indicates the uniform dispersion of Mxene on VOM-3, and high-quality homogeneous intercalated films can be obtained by spin-coating method.

Optical properties

Figure 4 shows the ex situ transmittance spectra of (a) V_2O_5 xerogel film, (b) VOM-1, (c) VOM-2, (d) VOM-3, (e) VOM-4, and (f) VOM-5 in the wavelength range of 300 to 800 nm at voltages of −1.0 V (colored state), 0.0 V and 1.0 V (bleached state). The films were subjected to polarization voltage for 30 s before measurement and the transmittance measured ex situ with the air as reference (baseline). The color change is the most visual manifestation of the electrochromic materials. The V_2O_5 xerogel film and VOM vary in color from light gray to yellow between voltages of −1.0 V and 1.0 V. All films in the bleached state show high transmittance in the spectral region of 500 ~ 800 nm, with a transmittance of about 80%. In the visible wavelength range (350 to 780 nm), the transmittance contrast (ΔT) for the V_2O_5 xerogel film, VOM-1, VOM-2, VOM-3, VOM-4, and VOM-5 at 372 nm were 7.70%, 23.36%, 43.46%, 49.03%, 38.77%, and 30.61%, respectively, which shows that the addition of Mxene increases the optical modulation range of the films. Among them, VOM-3 showed the maximum transmittance contrast (ΔT = 49.03%), which increased the range by about 6.37 times compared to V_2O_5 xerogel film transmittance contrast (ΔT = 7.70%). Therefore, VOM-3 was used as a target for subsequent characterization studies.

Figure 5 shows the energy gap (E_g) of V_2O_5 xerogel film and VOM-3. The E_g of the film satisfies the Tauc equation [41]: $(\alpha h\gamma)^{\frac{1}{2}} = A(h\gamma - E_g)$, where A is a constant, hγ is the energy of the incident photon and Eg is the energy gap. The E_g obtained by extrapolating linear fits to $(\alpha h\upsilon)^{1/2} = 0$. The E_g of V_2O_5 xerogel film is 2.15 eV, while the E_g of VOM-3 is 2.04 eV. The photon energy to cause intrinsic absorption must be equal to or greater than the E_g of the semiconductor. The smaller the E_g, the easier it is for the electrons to transition within the material. The reduction of the energy gap means that the electrons in the intercalation film are more likely to transition, which is beneficial for the redox reaction.

Electrochemical properties

Figure 6 shows the CV curves of (a) V_2O_5 xerogel film and (b) VOM-3 cycled 100 cycles between −1.0 V and 1.0 V at a scan rate of 50 mV/s. In the same potential region, the redox peaks of VOM-3 and V_2O_5 xerogel film are approximately similar. The three reduction peaks of the V_2O_5 xerogel film are at −0.54 V, −0.21 V, and 0.46 V, and the three oxidation peaks are at −0.29 V, 0.08 V, and 0.75 V. The three pairs of reduction peaks of VOM-3 are at −0.60 V, −0.29 V, and 0.51 V, and the three pairs of oxidation peaks are at −0.29 V, 0.17 V, and 0.68 V, respectively. The lithium ion insertion/extraction process is accompanied by a bleaching/coloring process and a reversible phase transition. Three pairs of redox peaks, corresponding to the three phases of the redox reaction, are related to the phase transition between the α, β, and γ phases of V_2O_5. The larger area of the CV curve for VOM-3 indicates a larger charge capacity and faster diffusion kinetics.

Figure 6 shows the results of cathodic (Q_c) and anodic (Q_a) charge densities of (c) V_2O_5 xerogel film and (d) VOM-3 during 100 cycles. The better cycling stability of VOM-3 (85.46% capacity retention after 100 cycles) compared to the V_2O_5 xerogel film (75.05% capacity retention after 100 cycles) is attributed to the good mechanical properties of Mxene, which buffer the volume expansion and inhibit the aggregation of V_2O_5 xerogel, suppressing the structural deformation of the film during cycling. This phenomenon is similar to the improved cycling stability of the composites due to V_2CT_x-Mxene doping with V_2O_5 xerogel [42].

Figure 7 shows the CA curves of (a) V_2O_5 xerogel film and (b) VOM-3. The response time, including both the coloring time and bleaching time, is defined as the time required for a 90% change of current [43]. The coloring time of the V_2O_5 xerogel film was 9.20 s and the bleaching time was 7.20 s. The coloring time of VOM-3 was 6.20 s (32.61% improvement) and the bleaching time was 3.20 s (55.56% improvement). This VOM-3 exhibited faster switching response in comparison to other vanadia systems.

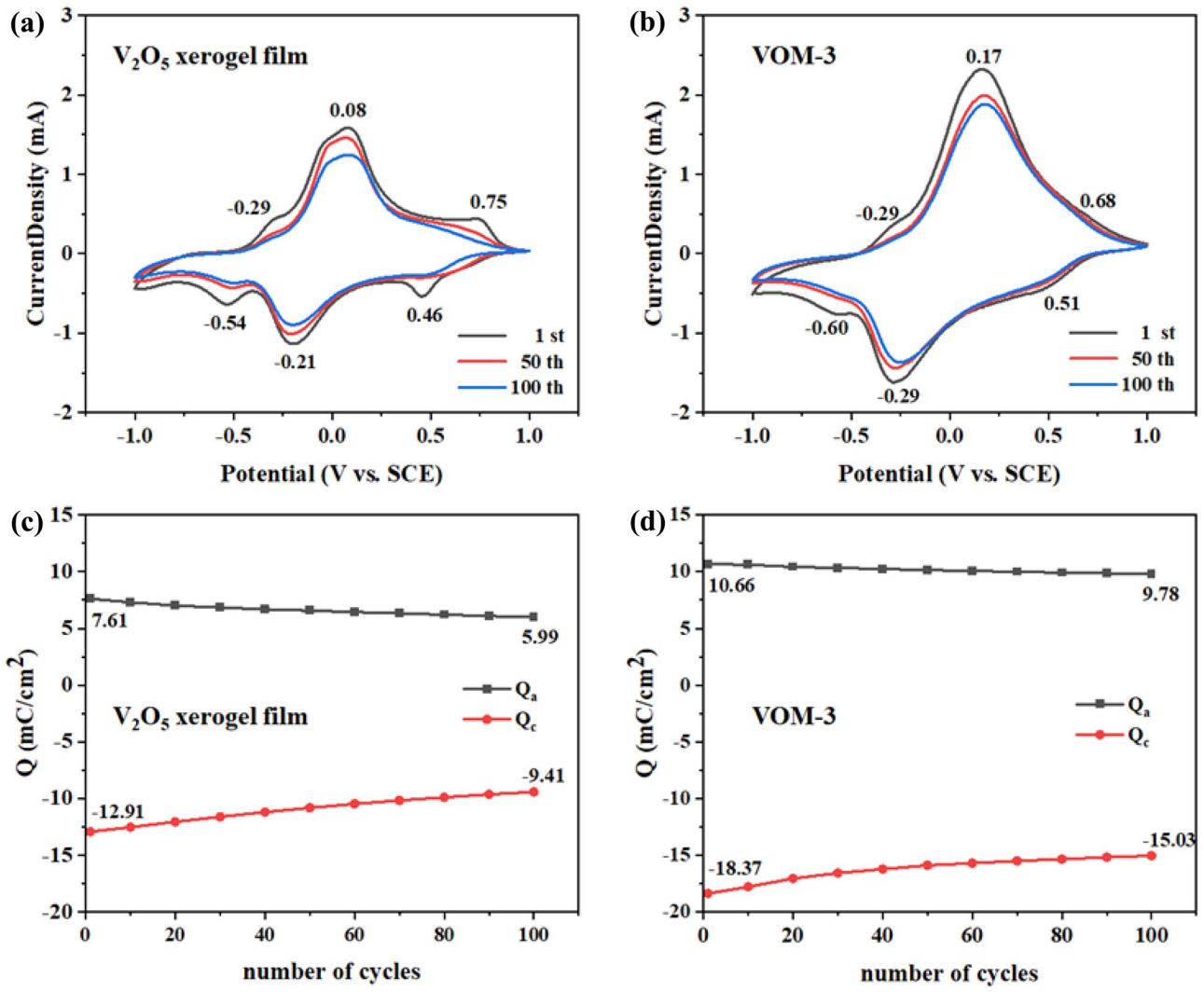

Fig. 6 CV curves of (**a**) V_2O_5 xerogel film and (**b**) VOM-3. Charge densities of (**c**) V_2O_5 xerogel film and (**d**) VOM-3

Tong et al. reported that the color-switching time of a V_2O_5 nanofiber film to be approximately 8.9 s for coloration and 7.4 s for bleaching [44]. Chang et al. reported that MoO_3/V_2O_5 hybrid nanobilayers prepared by sol–gel method and spin coating technique exhibited 8.2 s and 6.3 s for coloration and bleaching, respectively [45]. Karaca et al. prepared V_2O_5-PEDOT hybrid films with a coloring time of 10 s and a bleaching time of 14 s [46]. The faster response of VOM-3 is

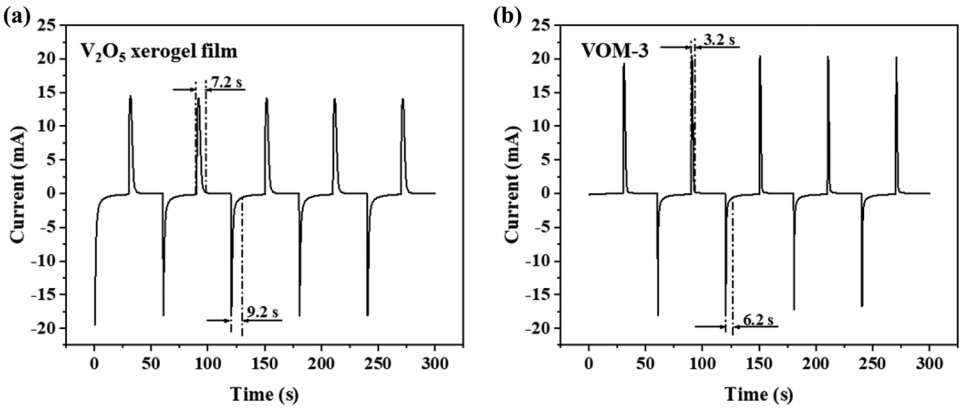

Fig. 7 CA curves of (**a**) V_2O_5 xerogel film and (**b**) VOM-3

due to the expanded electrical conductivity and layer spacing of Mxene in the film, which improves the diffusion coefficient of lithium ions.

Conclusion

In this article, V_2O_5 xerogel films and V_2O_5/Mxene intercalation films with electrochromic properties (yellow-green-light gray) were prepared by sol–gel method combined with spin coating technology. Compared with V_2O_5 xerogel films, VOM-3 shows a 1.12-fold increase in capacity retention after 100 cycles, a 0.57-fold increase in switching time, a 6.73-fold increase in transmittance contrast, and a 0.11 eV reduction in the energy gap. When 3% Mxene intercalated vanadium pentoxide xerogel, its electrochemical stability, response rate, and optical modulation range were improved, and V_2O_5/Mxene intercalated material was very attractive as an electrochromic material.

Supplementary information The online version contains supplementary material available at https://doi.org/10.1007/s10008-022-05171-5.

Funding This work was supported by the National Natural Science Foundation of China (No. 51472189), Henan key laboratory of special protective materials (Grant No. SZKJJ202101).

Declarations

Conflict of interest The authors declare no competing interests.

References

1. Platt JR (1961) Electrochromism, a possible change of color producible in dyes by an electric field. J Chem Phys 34:862–863. https://doi.org/10.1063/1.1731686
2. Rosseinsky DR, Mortimer RJ (2001) Electrochromic Systems and the Prospects for Devices. Adv Mater 13:783–793. https://doi.org/VanadiumPentoxide
3. Granqvist CG, Arvizu MA, Bayrak Pehlivan İ et al (2018) Electrochromic materials and devices for energy efficiency and human comfort in buildings: A critical review. Electrochim Acta 259:1170–1182. https://doi.org/10.1016/j.electacta.2017.11.169
4. Azens A, Granqvist C (2003) Electrochromic smart windows: energy efficiency and device aspects. J Solid State Electrochem 7:64–68. https://doi.org/10.1007/s10008-002-0313-4
5. Hou X, Wang Z, Pan J, Yan F (2021) Ionic liquid electrolyte-based switchable mirror with fast response and improved durability. ACS Appl Mater Interfaces 13:37339–37349. https://doi.org/10.1021/acsami.1c07438
6. Patel KJ, Bhatt GG, Ray JR et al (2017) All-inorganic solid-state electrochromic devices: a review. J Solid State Electrochem 21:337–347. https://doi.org/10.1007/s10008-016-3408-z
7. Yu H, Qi M, Wang J et al (2019) A feasible strategy for the fabrication of camouflage electrochromic fabric and unconventional devices. Electrochem Commun 102:31–36. https://doi.org/10.1016/j.elecom.2019.03.006
8. Zhang L, Xia G, Li X et al (2019) Fabrication of the infrared variable emissivity electrochromic film based on polyaniline conducting polymer. Synth Met 248:88–93. https://doi.org/10.1016/j.synthmet.2019.01.007
9. Mortimer RJ, Dyer AL, Reynolds JR (2006) Electrochromic organic and polymeric materials for display applications. Displays 27:2–18. https://doi.org/10.1016/j.displa.2005.03.003
10. Zhang W, Li H, Hopmann E, Elezzabi AY (2020) Nanostructured inorganic electrochromic materials for light applications. Nanophotonics 10:825–850. https://doi.org/10.1515/nanoph-2020-0474
11. Kumar R, Pathak DK, Chaudhary A (2021) Current status of some electrochromic materials and devices: a brief review. J Phys D: Appl Phys 54:503002. https://doi.org/10.1088/1361-6463/ac10d6
12. Yang G, Zhang Y-M, Cai Y et al (2020) Advances in nanomaterials for electrochromic devices. Chem Soc Rev 49:8687–8720. https://doi.org/10.1039/D0CS00317D
13. Rai V, Singh RS, Blackwood DJ, Zhili D (2020) A review on recent advances in electrochromic devices: a material approach. Adv Eng Mater 22:2000082. https://doi.org/10.1002/adem.202000082
14. Niu J, Wang Y, Zou X et al (2021) Infrared electrochromic materials, devices and applications. Appl Mater Today 24:101073. https://doi.org/10.1016/j.apmt.2021.101073
15. Barnes WH, Ahmed FR, Bachmann HG (1961) The crystal structure of vanadium pentoxide. Zeitschrift für Kristallographie 115:110–131. https://doi.org/10.1524/zkri.1961.115.1-2.110
16. Tadeu Cestarolli D, Maria Guerra E (2021) Vanadium pentoxide (V_2O_5): Their obtaining methods and wide applications. In: Haider S, Haider A (eds) Transition Metal Compounds - Synthesis, Properties, and Application. IntechOpen
17. Coustier F, Hill J, Owens BB et al (1999) Doped vanadium oxides as host materials for lithium intercalation. J Electrochem Soc 146:1355–1360. https://doi.org/10.1149/1.1391770
18. Legendre J-J, Livage J (1983) Vanadium pentoxide gels: J Colloid Interface Sci 94:75–83. https://doi.org/10.1016/0021-9797(83)90236-9
19. Potiron E, Salle LG, Verbaere A et al (1999) Electrochemically synthesized vanadium oxides as lithium insertion hosts. Electrochim Acta 45:197–214. https://doi.org/10.1016/S0013-4686(99)00204-2
20. Lantelme F, Mantoux A, Groult H, Lincot D (2003) Electrochemical Study of Phase Transition Processes in Lithium Insertion in V2O5 Electrodes. J Electrochem Soc 150:A1202–A1208. https://doi.org/10.1149/1.1595658
21. Koo B-R, Bae J-W, Ahn H-J (2019) Percolation effect of V2O5 nanorod/graphene oxide nanocomposite films for stable fast-switching electrochromic performances. Ceram Int 45:12325–12330. https://doi.org/10.1016/j.ceramint.2019.03.148
22. Hsiao Y-S, Chang-Jian C-W, Syu W-L et al (2021) Enhanced electrochromic performance of carbon-coated V2O5 derived from a metal–organic framework. Appl Surf Sci 542:148498. https://doi.org/10.1016/j.apsusc.2020.148498
23. Xiong C, Aliev AE, Gnade B, Balkus KJ (2008) Fabrication of silver vanadium oxide and V_2O_5 nanowires for electrochromics. ACS Nano 2:293–301. https://doi.org/10.1021/nn700261c
24. Cholant CM, Westphal TM, Balboni RDC et al (2017) Thin films of V2O5/MoO3 and their applications in electrochromism. J Solid State Electrochem 21:1509–1515. https://doi.org/10.1007/s10008-016-3491-1
25. Ravi R, Surendren S, Deb B (2021) Studies on all-solid electrochromic devices fabricated by a bilayered assembly of hydrated vanadium pentoxide and PEDOT:PSS Coatings. Surfaces and Interfaces 22:100860. https://doi.org/10.1016/j.surfin.2020.100860
26. Huguenin F, dos Santos DS, Bassi A et al (2004) Charge storage capability in nanoarchitectures of V2O5/chitosan/poly(ethylene

oxide) produced using the layer-by-layer technique. Adv Funct Mater 14:985–991. https://doi.org/10.1002/adfm.200305077
27. Naguib M, Kurtoglu M, Presser V et al (2011) Two-dimensional nanocrystals produced by exfoliation of Ti3AlC2. Adv Mater 23:4248–4253. https://doi.org/10.1002/adma.201102306
28. Anasori B, Lukatskaya MR, Gogotsi Y (2017) 2D metal carbides and nitrides (MXenes) for energy storage. Nat Rev Mater 2:16098. https://doi.org/10.1038/natrevmats.2016.98
29. Pang J, Mendes RG, Bachmatiuk A et al (2019) Applications of 2D MXenes in energy conversion and storage systems. Chem Soc Rev 48:72–133. https://doi.org/10.1039/C8CS00324F
30. Verger L, Natu V, Carey M, Barsoum MW (2019) MXenes: an introduction of their synthesis, select properties, and applications. Trends in Chemistry 1:656–669. https://doi.org/10.1016/j.trechm.2019.04.006
31. Kshetri T, Tran DT, Le HT et al (2021) Recent advances in MXene-based nanocomposites for electrochemical energy storage applications. Prog Mater Sci 117:100733. https://doi.org/10.1016/j.pmatsci.2020.100733
32. Xu G, Zhang Y, Gong Z et al (2021) Three-dimensional hydrated vanadium pentoxide/MXene composite for high-rate zinc-ion batteries. J Colloid Interface Sci 593:417–423. https://doi.org/10.1016/j.jcis.2021.02.090
33. Wang Y, Lubbers T, Xia R et al (2021) Printable two-dimensional V $_2$ O $_5$ /mxene heterostructure cathode for lithium-ion battery. J Electrochem Soc 168:020507. https://doi.org/10.1149/1945-7111/abdef2
34. Mahmood M, Zulfiqar S, Warsi MF et al (2022) Nanostructured V2O5 and its nanohybrid with MXene as an efficient electrode material for electrochemical capacitor applications. Ceram Int 48:2345–2354. https://doi.org/10.1016/j.ceramint.2021.10.014
35. Alonso B, Livage J (1999) Synthesis of vanadium oxide gels from peroxovanadic acid solutions: a 51V NMR study. J Solid State Chem 148:16–19. https://doi.org/10.1006/jssc.1999.8283
36. Cai Y, Shen J, Ge G et al (2018) Stretchable Ti3C2Tx MXene/carbon nanotube composite based strain sensor with ultrahigh sensitivity and tunable sensing range. ACS Nano 12:56–62. https://doi.org/10.1021/acsnano.7b06251
37. Petkov V, Trikalitis PN, Bozin ES et al (2002) Structure of V2O5·nH2O xerogel solved by the atomic pair distribution function technique. J Am Chem Soc 124:10157–10162. https://doi.org/10.1021/ja026143y
38. Wan Z, Darling RB, Anantram MP (2015) Programmable diode/resistor-like behavior of nanostructured vanadium pentoxide xerogel thin film. Phys Chem Chem Phys 17:30248–30254. https://doi.org/10.1039/C5CP04755B
39. Bera B, Esther ACM, Dey A, Mukhopadhyay AK (2016) Structural, optical and electrical properties of V2O5 xerogel thin films. Indian J Phys 90:687–692. https://doi.org/10.1007/s12648-015-0807-4
40. Silversmit G, Depla D, Poelman H et al (2004) Determination of the V2p XPS binding energies for different vanadium oxidation states (V5+ to V0+). J Electron Spectrosc Relat Phenom 135:167–175. https://doi.org/10.1016/j.elspec.2004.03.004
41. Tauc J, Grigorovici R, Vancu A (1966) Optical properties and electronic structure of amorphous germanium. Phys Stat Sol (b) 15:627–637. https://doi.org/10.1002/pssb.19660150224
42. Venkatkarthick R, Rodthongkum N, Zhang X et al (2020) Vanadium-based oxide on two-dimensional vanadium carbide MXene (V_2O_x @ V_2CT_x) as cathode for rechargeable aqueous zinc-ion batteries. ACS Appl Energy Mater 3:4677–4689. https://doi.org/10.1021/acsaem.0c00309
43. Zhang J, Wang XL, Xia XH et al (2010) Enhanced electrochromic performance of macroporous WO3 films formed by anodic oxidation of DC-sputtered tungsten layers. Electrochim Acta 55:6953–6958. https://doi.org/10.1016/j.electacta.2010.06.082
44. Tong Z, Lv H, Zhang X et al (2015) Novel morphology changes from 3D ordered macroporous structure to V2O5 nanofiber grassland and its application in electrochromism. Sci Rep 5:16864. https://doi.org/10.1038/srep16864
45. Chang C-C, Chi P-W, Chandan P, Lin C-K (2019) Electrochemistry and rapid electrochromism control of MoO3/V2O5 hybrid nanobilayers. Materials 12:2475. https://doi.org/10.3390/ma12152475
46. Karaca GY, Eren E, Alver C et al (2017) Plasma modified V2O5/PEDOT hybrid based flexible electrochromic devices. Electroanalysis 29:1324–1331. https://doi.org/10.1002/elan.201600631